frontiers | Frontiers in Materials

TYPE Original Research
PUBLISHED 03 August 2022
DOI 10.3389/fmats.2022.935096

OPEN ACCESS

EDITED BY
Boguang Yang,
The Chinese University of Hong Kong, China

REVIEWED BY
Jie Gao,
Second Military Medical University, China
Zhiwei Fang,
Johns Hopkins University, United States

*CORRESPONDENCE
Xiufeng Xiao,
xfxiao@fjnu.edu.cn
Yongqi Shan,
yongqishan@126.com

†These authors have contributed equally to this work

SPECIALTY SECTION
This article was submitted to Biomaterials, a section of the journal Frontiers in Materials

RECEIVED 03 May 2022
ACCEPTED 04 July 2022
PUBLISHED 03 August 2022

CITATION
Chen H, Liao R, Du Q, Li C, Xiao X and Shan Y (2022), Injectable hyaluronic acid/oxidized chitosan hydrogels with hypochlorous acid released for instant disinfection and antibacterial effects. *Front. Mater.* 9:935096. doi: 10.3389/fmats.2022.935096

Injectable hyaluronic acid/oxidized chitosan hydrogels with hypochlorous acid released for instant disinfection and antibacterial effects

Han Chen[1†], Ran Liao[2†], Qianqian Du[3], Cong Li[3], Xiufeng Xiao[4*] and Yongqi Shan[1*]

[1]Department of Pharmacy, Department of General Surgery, The General Hospital of Northern Theater Command, Shenyang, China, [2]Department of Urology, The Second Affiliated Hospital of Chengdu Medical College (China National Nuclear Corporation 416 Hospital), Chengdu, China, [3]Department of Biomaterial, College of Life Sciences, Mudanjiang Medical University, Mudanjiang, China, [4]College of Chemistry and Materials Science, Fujian Provincial Key Laboratory of Advanced Materials Oriented Chemical Engineering, Fujian Normal University, Fuzhou, China

Bacterial infections of wounds significantly increase the occurrence of complications, which have become a public health problem and pose a serious threat to human health. Therefore, an ideal wound dressing should not only possess suitable mechanical strength and a moist environment, but also instant disinfection and antibacterial properties. Owing to their high water content and permeability, hydrogels have great potential for the application in wound dressing. In this study, we developed an injectable hyaluronic acid (HA)/oxidized chitosan (OCS) hydrogel with good biocompatibility, self-healing, and tissue adhesive properties. Moreover, the slow release of micro hypochlorous acid (HClO), which is a common bactericide during hydrogel formation, can lead to instant disinfection; and the positive charge of OCS in this hydrogel can achieve a sustainable antibacterial effect. Thus, this hydrogel is a promising wound dressing material in clinical treatments.

KEYWORDS

hydrogel, injectable, hypochlorous acid, antibacterial effects, biocompatibility

Introduction

Bacteria are highly adaptable and ubiquitous in natural environments and bacterial infections of wounds are quite common in daily life (Li et al., 2018; Ahmed et al., 2020; Jamaledin et al., 2020). For instance, skin injuries caused by mechanical damage, undesirable temperatures, and chemicals are easily infected by bacteria when one fails to clean potentially infectious microbiological and necrotic tissues in time. Currently, various antibacterial strategies have been proposed, including photodynamic antimicrobial therapy (Hu et al., 2019; Chandna et al., 2020), hydrophilic antifouling coatings (Knowles et al., 2017; Tian et al., 2019), and metallic nanomaterials (Vimbela

et al., 2017; Rehman et al., 2018). However, the aforementioned strategies also have some limitations, such as the complex operation and release of harmful ions. Therefore, it is still a challenge to develop a convenient wound dressing material with effective antibacterial properties.

The process of wound healing provides the inspiration for antibacterial wound dressing design (Makvandi et al., 2019; Zhang et al., 2019). Wound healing, a complex process of natural restoration and tissue growth progression, involves the following four different phases: the coagulation and hemostasis phase, inflammatory phase, proliferation period, and maturation phase (Derakhshanfar et al., 2019; Abdollahi et al., 2021). These phases must occur in a proper sequence and penetrate each other in a well-connected cascade to create optimal wound healing. The pathological conditions of the wound and the type of dressing material significantly affect the progress of these phases. Inspired by the progress of moist wound healing, we envision hydrogels to be the ideal wound dressing material because of their three-dimensional (3D) polymer network structure, which is similar to an extracellular matrix (Smithmyer et al., 2014; Gaspar-Pintiliescu et al., 2019). Owing to their excellent biocompatibility, absorption capability, and biodegradability, natural polymers containing alginate (Aikawan et al., 2015; Emami et al., 2018; Zhang et al., 2018), collagen (Cho et al., 2017; Wakuda et al., 2018; Lin et al., 2019), chitosan (CS) (Wang et al., 2018; Shariatinia, 2019; Bagheri et al., 2021), and hyaluronic acid (HA) (Li et al., 2018; Zhu et al., 2018; Kim et al., 2019; Wolf and Kumar, 2019), derived from animals, plants, and microorganisms are widely used to prepare antibacterial hydrogels applied in wound dressings.

CS is the product of the *N*-deacetylation of chitin with widespread applications in biomaterials owing to its non-toxicity, ease of modification, and antibacterial activity. Its unique antibacterial effect is based on the abundant positively charged primary amine groups, garnering increasing attention from researchers in the design of CS-derived antibacterial biomaterials. Bagheri et al., designed and fabricated CS/polyethylene oxide (PEO) nanofibers conjugated with antibacterial silver and zinc oxide nanoparticles. These nanocomposites showed a good antioxidant effect and antibacterial activity against *S. aureus*, *E. coli*, and *P. aeruginosa* (Bagheri et al., 2021). For the application of CS, its poor water solubility is the main obstacle (Pellá et al., 2018). Fortunately, the oxidation of CS can solve this problem and simultaneously provide CS with a new reactivity. Another natural polymer, HA, is an acidic glycosaminoglycan consisting of *N*-acetyl-D-glucosamine and D-glucuronic acid units. Because HA has super water absorption and retention properties, HA has been applied in a wide range from cosmetic materials to bioengineering scaffolds (Litwiniuk et al., 2016; Park et al., 2019).

Recently, diverse injectable antibacterial hydrogels have been developed using various methods, such as physical crosslinking (hydrogen bond, hydrophobic interactions, and electrostatic interactions) (Shao et al., 2017; Deng et al., 2018; Liang et al., 2019; Wang J et al., 2020), and chemical crosslinking (Michael addition, Schiff-base reaction, and click reaction) (Jalalvandi et al., 2017; Huang et al., 2018; Du et al., 2019; Pupkaite et al., 2019; Pérez-Madrigal et al., 2020). The Schiff-base reaction has primarily garnered particular interest owing to its short gelling time and gentle gelling condition. Therefore, we designed and prepared this hydrogel, which is based on the Schiff-base reaction of oxidized chitosan (OCS) and hydrazine-modified HA (HA-ADH). Although hypochlorous acid (HClO) is an efficient antibacterial agent (Chen et al., 2016; Raval, et al., 2021), it is limited in application to clinical treatment owing to its instability. To address this issue, we utilized the reaction between calcium hypochlorite and salicylic acid to produce hypochlorous acid along with the formation of the hydrogel. During hydrogel formation, through the mixing of OCS and HA-ADH solutions, HClO is released simultaneously owing to the reaction between salicylic acid (SA) and calcium hypochlorite that are previously dissolved in the OCS and HA-ADH solutions, respectively.

In this article, we present a novel hydrogel system that can *in situ* gel on the surface of a wound to be used as an antibacterial wound dressing material. This new hydrogel dressing is able to achieve a desirable "instant disinfection and antibacterial" therapeutic effect. Moreover, this hydrogel shows good biocompatibility, mechanical, and tissue-adhesive properties. All these characterizations demonstrate that this hydrogel has great potential to be used as an antibacterial wound dressing material to accelerate wound healing.

Experimental

Materials

Chitosan (CS, molecular mass of ~50 kDa, deacetylation degree of 95%), sodium periodate ($NaIO_4$ ≥99.0%), N-(3-Dimethylaminopropyl)-N′-ethylcarbodiimide hydrochloride (EDC), sodium hydroxide (NaOH), agarose, methylene blue, methyl orange, and propidium iodide (PI) were purchased were purchased from Macklin and were used directly. Sodium hyaluronate (HA, molecular mass of 92000 Da) was purchased from Shandong Focuschem Biotech Co., Ltd. 1-Hydroxybenzotriazole (HOBt) and adipic acid dihydrazide (ADH) were purchased from J&K Chemical. PBS (pH = 7.4), fetal bovine serum (FBS), penicillin–streptomycin (PS) solution, Dulbecco's modified Eagle medium (DMEM) L-glutamine, and calcein AM were purchased from Gibco Co., Ltd. (Carlsbad, CA, Uniteed States).

Synthesis and characterization of OCS

For the synthesis of OCS, 2 g chitosan was first dissolved in 200 ml 0.5 wt% dilute glacial acetic acid aqueous solution. 1.325 g

sodium periodate ($NaIO_4$) was added into the mixture to oxide the chitosan polymer. The reaction was stirred for 24 h in the dark at room temperature. Subsequently, the mixture solution was dialyzed against deionized water (DI water) for 4 days to remove the unreacted small $NaIO_4$ molecule (14 kDa cutoff dialysis membrane). The obtained purified product was freeze-dried by a lyophilizer and stored at −20°C in the freezer. The OCS samples were analyzed by Fourier transform infrared (FT-IR) spectroscopy. In detail, the KBr pellet method was used in the range of 500–4,000 cm^{-1} at 25°C, recorded with a Nicolet 5700 spectrophotometer (Thermo Fisher Scientific Inc., MA).

Synthesis and characterization of HA-ADH

First, 2 g of HA (M = 920000 Da) was dissolved in 200 ml of the buffer solution (pH = 6.5). Afterward, 2.5 g EDC and 1.78 g HOBT were added into the HA solution and kept stirring at room temperature. After 1 h, 9 g adipic dihydrazide (ADH) was added into the mixture solution and the reaction was further stirred and kept for 24 h at room temperature to obtain the crude product. The product was purified against DI water for 4 days by a dialysis membrane (14 kDa cutoff dialysis membrane), and the product was lyophilized, and then stored at- 20°C in the freezer. The HA-ADH samples were also analyzed by Fourier transform infrared (FT-IR) spectroscopy with a similar protocol as that of OCS.

Preparation of injectable OCS/HA hydrogels

An injectability test was performed as described (Makvandi et al., 2019; Makvandi et al., 2021). In the first step, the HA-ADH solution and OCS solution was prepared separately by dissolving in PBS at different concentrations. Then, these two solutions were subsequently mixed at a volume ratio of 1:1 by using a double-barrel syringe. The hydrogels with different component concentrations were labeled as OCS_x/HA hydrogels meaning that the concentration of HA-ADH was fixed at 3% and the concentration of OCS was signed as y % (4%, 5%, 6%, and 7%).

Preparation of injectable OCS/HA-HClO hydrogels

Based on the preparation of the OCS/HA hydrogel, we further developed the OCS/HA-HClO hydrogel. Briefly, HA-ADH was dissolved in the PBS buffer with 125 mg/L of a $Ca(ClO)_2$ solution and OCS was dissolved in the PBS buffer of 2.5 mM salicylic acid (SA), respectively. Then, these two precursor solutions were added into the two independent cavities of the double-barrel syringe. Through the mixed injection of these prepared two solutions into models or in the surface of skin with the volume ratio of 1:1, a series of OCS/HA-HClO hydrogels was formed with the *in situ* gelation method.

Gelation time test of the OCS/HA hydrogels

The gelation time was measured by a tube-inversion method (Jommanee et al., 2018; Wang Y et al., 2020). Briefly, HA-ADH and OCS were separately dissolved in the PBS solution. These two kinds of solutions were mixed with a double-barrel syringe to obtain the HA/OCS hydrogels, and the gel time was denoted as the time when the hydrogels showed no ability to flow. The gel time of OCS/HA-HClO hydrogel was determined by a similar method.

Swelling ratio measurement of the OCS/HA hydrogels

To evaluated the swelling kinetics behavior of the OCS/HA hydrogels, all samples (100 μL, $n = 5$) were prepared in a PTFE mold (10 mm in diameter, 1 mm in height), respectively. All samples were immersed in 500 μl of the PBS buffer for 24 h at room temperature. Then, the hydrogels were removed from the PBS buffer and weighted at specific time intervals (0.5, 1, 3, 7, 12, and 24 h) after removing the liquid around the samples. This weight was marked as W_s. Hydrogels were subsequently freeze-dried to obtain the dry weight (W_d).

The following formulation is used to calculate the swelling ratio of hydrogels:

$$\text{Swelling ratio}\,(\%) = \frac{W_s - W_d}{W_d} \times 100\%.$$

Degradation properties' measurement of hydrogels

The degradation rate of hydrogels was also characterized. OCS_4/HA, OCS_5/HA, OCS_6/HA, and OCS_7/HA (100 μl, $n = 5$) were immersed in 1 ml of the PBS buffer for 12 h at room temperature to reach the swelling equilibrium. We marked this time point as 0 h and the weight of the hydrogel samples were recorded as W0. Then, these swelled hydrogel samples were immersed in 1 ml PBS buffer at 37°C for the degradation test. At specific time intervals (1, 4, 10h, 1d, 2d, 4d, and 7d), the hydrogel samples were weighed as W1. Therefore, the degradation remaining ratio was calculated as W1/W0 × 100%.2.9 Rheological test of hydrogels.

All rheological experiments were carried out on a TA Discovery DHR-2 rheometer equipped with a parallel plate with an 8 mm diameter and a 1 mm gap size at 25°C. Oscillation strain sweep was performed with fixed oscillation frequency 1 Hz and variable applied strain from 1 % to 1,000%.

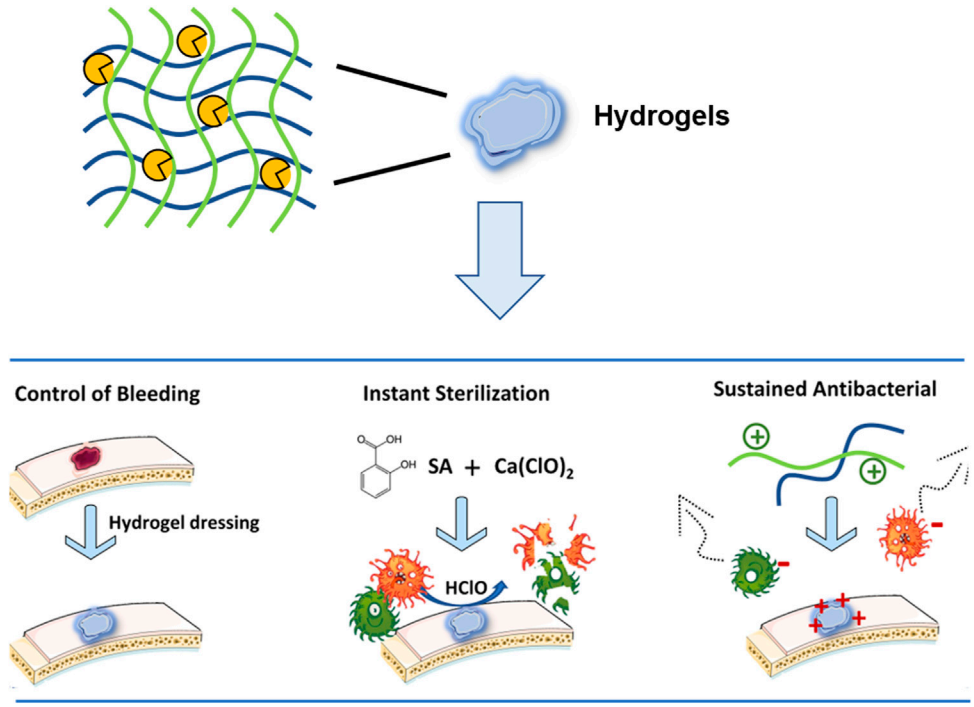

SCHEME 1
Scheme of the antibacterial activity of the OCS/HA-HClO hydrogel.

Alternating strain sweep was measured with a fixed oscillation frequency of 1 Hz and sequential strains with 1% (100 s) and 500% (100 s) for 3 cycles.

Self-healing, injectable, and tissue-adhesive properties' observation

The self-healing, injectable, and adhesion behaviors were measured by a macroscopic experiment. In detail, in order to test the self-healing performance of hydrogels, two triangular pieces (10 mm sides, 1 mm thickness) of a hydrogel were stained with methylene blue and methyl orange, respectively. These behaviors of hydrogels were monitored by digital photographs with specific time intervals. As for the injectable behavior test, the dyed hydrogel is directly injected into the PVC mold of the pentacle successively. Porcine skin was purchased to test the adhesive of the hydrogel, and the hydrogel was stained with methylene blue.

In Vitro antibacterial activity test of hydrogels

E. coli (Gram-negative) and *S. aureus* (Gram-positive) were used to assess the antibacterial activity of hydrogels. Antibacterial activity of the OCS/HA hydrogel and the OCS/HA-HClO hydrogel were evaluated *in vitro* by agar plate diffusion tests. During antibacterial activity tests, the OCS/HA hydrogel and the OCS/HA-HClO hydrogel were selected as the experimental groups. Then the as-prepared bacterial suspensions, which contained approximately 1×10^6 CFU ml^{-1}, were added into the following groups: 1) PBS buffer (990 μl); 2) agarose hydrogel coated 48-well plate; 3) OCS/HA hydrogel coated 48-well plate; 4) OCS/HA-HClO hydrogel coated 48-well plate; and 5) penicillin–streptomycin (PS) solution (990 μL). All samples were incubated at 37°C for 2 h, and the bacterial was re-suspended in 1 ml of PBS buffer. The diluent bacterial suspension solution (10^4 CFU ml^{-1}) was seeded onto the Luria-Bertani (LB) agar surface and then incubated for 24 h at 37°C. The samples were measured with macroscopic digital photographs.

In Vitro biocompatiblity test of hydrogels

In order to test the biocompatibility of our OCS/HA-HClO and OCS/HA-HClO hydrogels, we used 3T3 cells as the model cells. The OCS/HA and OCS/HA-HClO hydrogels (total volume for per hydrogel is 200 μl, $n = 4$) were formed in the bottom of 24-well plates, respectively. Then, 1 ml of a growth media containing 2×10^5 3T3 cells were added into the 24-well plate. After 2 d or 5 d of culture, the OCS/HA and OCS/HA-HClO hydrogels were taken out

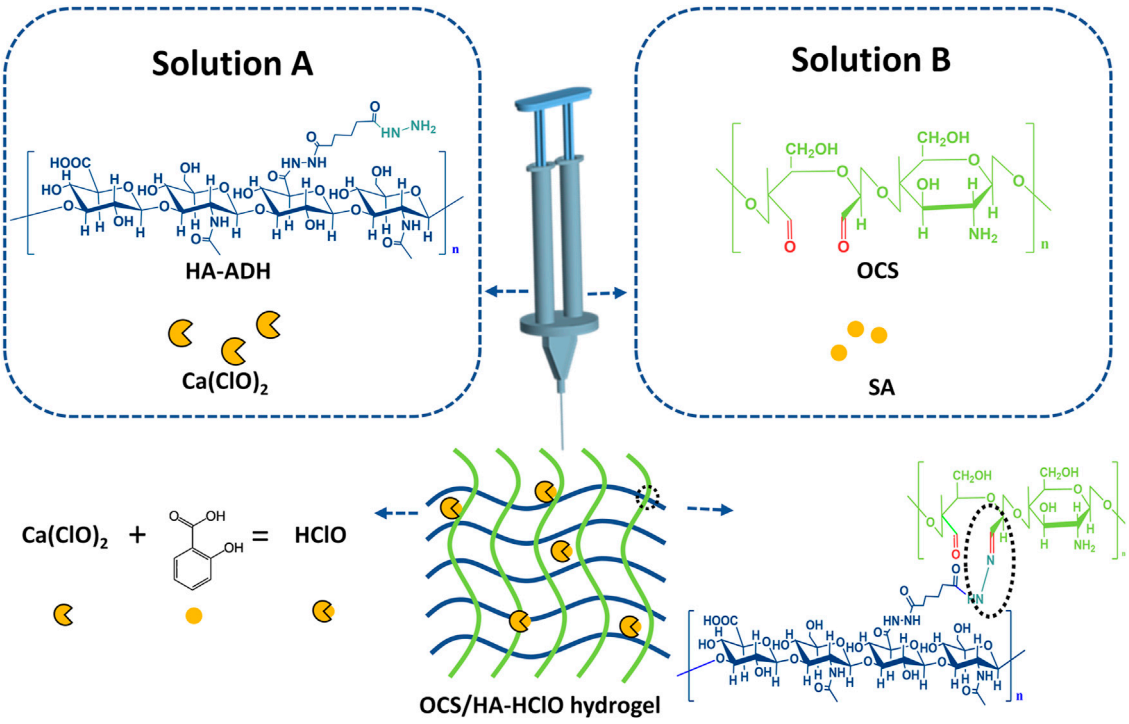

FIGURE 1
Fabrication of the OCS/HA-HClO hydrogel based on the reversible Schiff-based reaction.

from the 24-well plate to test the cell viability of 3T3 cells on the surface of the hydrogels by live/dead staining.

After 2 d or 5 d of culture as described previously, the cell viability assay was performed. The cells were cultured without hydrogels as the control group. 90 μl culture medium of each group was taken out and added into the 96-well plates. Then, 10 μl of a CCK-8 kit solution was added to each well and the plates were incubated at 37°C for about 2 h. Next, a microplate reader was used to measure the optical density (OD) at 450 nm. The survival rate of cells = (experimental group OD value—blank group OD value)/(control group OD value—blank group OD value).

Results and discussion

Fabrication of the OCS/HA-HClO hydrogels

In this study, we developed an injectable, self-healing, bioadhesive, and antibacterial hydrogel that is based on the natural polymer materials of CS and HA to overcome the challenge of covering irregular wounds and subsequently providing an antibacterial protection of the wounds (Scheme 1 and Figure 1).

The synthetic routes of HA-ADH and OCS are shown in Figures 2A,B. HA was conjugated with ADH in the presence of EDC and HOBT. CS reacted with $NaIO_4$ to form the OCS. The successful modification of natural HA and CS polymers was then characterized by Fourier transform infrared (FT-IR) spectroscopy. Compared with HA, the FT-IR spectra of the HA-ADH shows characteristic peaks at 1,130 cm^{-1} that are attributed to the hydrazide group, indicating that HA-ADH was successfully prepared (Figure 2C). In the FT-IR spectra of OCS, the clear peaks at 2,900 and 3,010 cm^{-1} indicate the satisfactory formation of the aldehyde groups in the OCS backbone (Figure 2D). Two types of precursor solutions were obtained by dissolving HA-ADH and OCS in $Ca(ClO)_2$ and SA solutions, respectively. Notably, the acidity of SA can improve the solubility of OCS. The prepared solution A (HA-ADH/$Ca(ClO)_2$ solution) and the solution B (OCS/SA solution) were separately sucked into two independent syringes. We used a tee cock valve to connect these two syringes and a 27G needle, and subsequently performed the mixing injection to form the OCS/HA-HClO hydrogel on the surface of the wound directly. This hydrogel is mildly but rapidly formed within minutes after mixing (Supplementary Figure S1 and Supplementary Table S1). As shown in Supplementary Figure S1, the gelation time decreases accompanied by the increase of the OCS concentration. The crosslinkings of the OCS/HA-HClO hydrogel are formed based on the spontaneous Schiff-base reaction of the aldehyde groups in OCS and the hydrazide

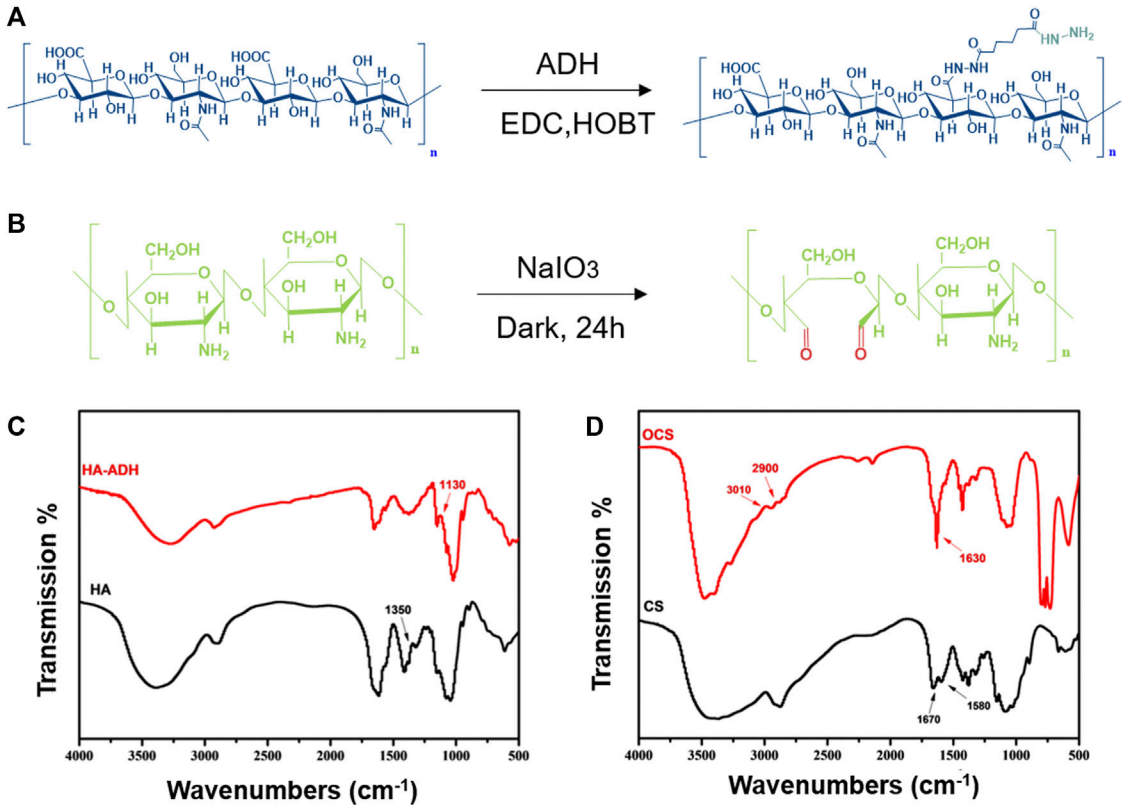

FIGURE 2
Fabrication and structural characterization of HA-ADH and OCS. The synthetic route of **(A)** HA-ADH and **(B)** OCS. FT-IR spectra of **(C)** HA, HA-ADH, **(D)** CS, and OCS.

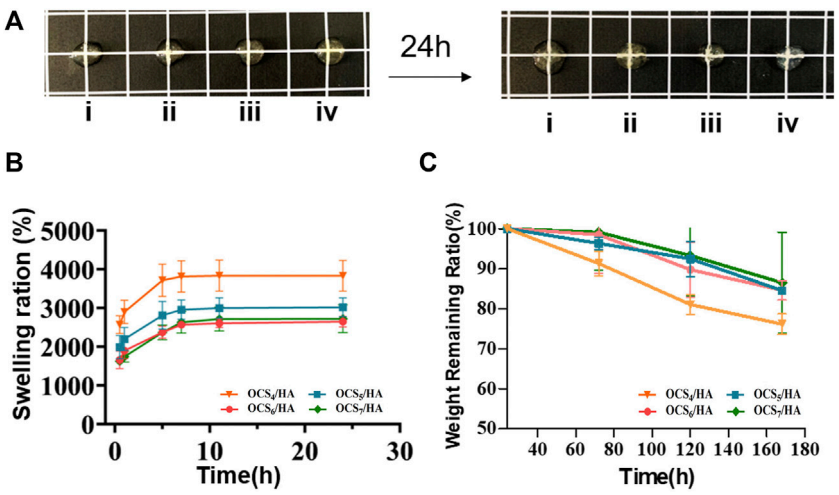

FIGURE 3
Swelling and degradation properties of the OCS/HA hydrogels with different OCS concentrations. **(A)** Photographic illustration of the OCS/HA hydrogels before and after reaching swelling equilibrium in a phosphate-buffered saline (PBS) buffer after 24 h: (i) OCS_4/HA, (ii) OCS_5/HA, (iii) OCS_6/HA, and (iv) OCS_7/HA. The square grid is 1 × 1 cm. **(B)** Swelling profiles of OCS/HA hydrogels over 24 h in PBS at 37°C. **(C)** Degradation ratio of the OCS/HA hydrogel in PBS at 37°C for 7 days *in vitro*.

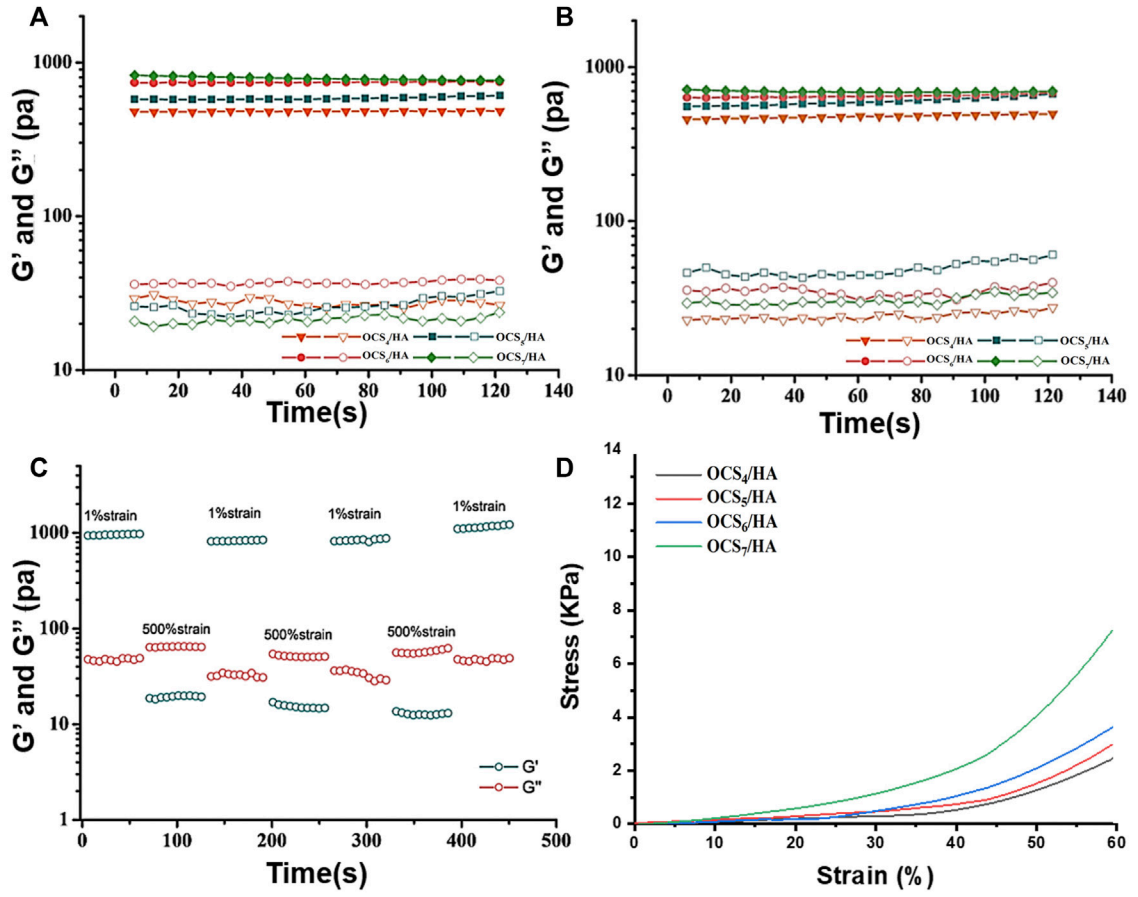

FIGURE 4
Rheological properties of the OCS/HA hydrogels. Time sweep measurements of the **(A)** OCS/HA hydrogel and the **(B)** OCS/HA-HClO hydrogel. **(C)** Alternating strain sweep of the OCS_7/HA-HClO hydrogel with a low strain at 1% and a high strain at 500%. **(D)** Compressive test of the OCS/HA hydrogel.

groups in HA-ADH. Simultaneously, the predissolved $Ca(ClO)_2$ in solution A and SA in solution B react with each other to release bactericide HClO (Scheme 1). The fresh HClO functions as an oxidizer to oxidate the protein on the surface of the bacteria to timely kill the bacteria in the wound. After the instant disinfection, the positive charges of the OCS/HA-HClO hydrogels from the protonated amino groups of OCS provide antibacterial protection for the wound. During gelation, some aldehyde groups of OCS also react with the amino groups of the wound tissue, such that the OCS/HA-HClO hydrogel can adhere to the wound tightly to offer all-around protection for the wound.

Swelling and degradation profiles of the OCS/HA hydrogels

Comparing the photographs of the OCS/HA hydrogels before and after immersing in the PBS buffer for 24 h, we discovered that the swelling ratio of the OCS/HA hydrogel decreases with increasing OCS concentration (Figure 3A). The swelling profile of this series of OCS/HA hydrogels in Figure 3B also indicates this phenomenon and further shows that when the OCS concentration is greater than 6%, the swelling ratio remains basically unchanged at 1.5 times of the hydrogels' original weights. All groups of the OCS/HA hydrogels reach the swelling equilibrium after soaking for 10 h in PBS, demonstrating the good water-absorbing quality of the OCS/HA hydrogels. Therefore, the OCS/HA hydrogel is able to absorb the exudate promptly and efficiently. Furthermore, the degradation behavior was determined in Figure 3C. The degradation rate of hydrogels decreases with the increase in the OCS concentration and reaches the maximum value when the OCS concentration exceeds 6%. The aforementioned results indicate that the changing trends of the swelling ratio and degradation speed are highly similar. This is because both the swelling and degradation behaviors are closely related to the

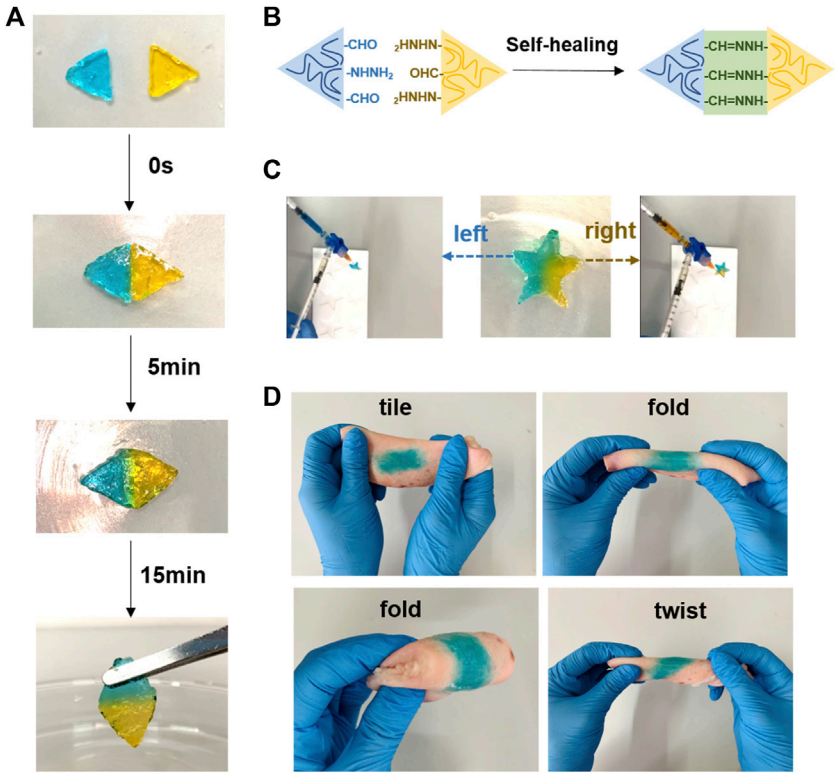

FIGURE 5
Self-healing, injection, and adhesion performance of the OCS/HA-HClO hydrogels. **(A)** Photo illustration of the self-healing process. **(B)** Schematic of self-healing of the OCS/HA-HClO hydrogels. Photo illustration of **(C)** injection and **(D)** adhesion of hydrogels.

crosslinking density of the hydrogel. A high crosslinking density implies a dense 3D hydrogel structure that prevents the permeation of water into the hydrogel and the degradation of the hydrogel framework. Therefore, these results illustrate that the crosslinking density of the OCS/HA hydrogel is improved through the increment in the OCS concentration and does not change after the OCS concentration reaches 6%. This is because the hydrazide group number of HA-ADH is more than the aldehyde group number of OCS in OCS_4/HA and OCS_5/HA groups, and the excess OCS can lead to the further formation of crosslinkings. When the OCS concentration was raised to 6%, all hydrazide groups of HA-ADH were utilized to form crosslinkings; thus, a further increment of OCS concentration did not affect the crosslinking density of the OCS/HA hydrogel.

Rheological properties of the OCS/HA and OCS/HA-HClO hydrogels

The time sweep results of OCS/HA in Figure 4A show that the storage modulus (G′) is higher than the loss modulus (G″) for all groups of the OCS/HA hydrogels, demonstrating the successful gelation of the OCS/HA hydrogels. It also proves that the increasing amount of OCS in the OCS/HA hydrogels leads to the increment of both G′ and G″ until the OCS concentration reaches 6% (Figure 4A). Therefore, the changing trend of the modulus is similar to those of the swelling and degradation ratios. This finding confirms our speculation that when the OCS concentration reaches 6%, all the hydrazide groups of HA-ADH are consumed to form the crosslinking inside the hydrogel; thus, increasing the OCS concentration to 7% no longer improves the modulus of the OCS/HA hydrogels. We subsequently performed the rheological time sweep test for the OCS/HA-HClO hydrogels. The results prove that the addition of SA and $Ca(ClO)_2$ has no negative effects on the formation of hydrogels (Figure 4B). Considering the swelling ratio, degradation rate, and rheological modulus results, we selected the OCS_7/HA-HClO hydrogel for all the subsequent tests. Accordingly, the redundant aldehyde groups of OCS can react with the amino groups of wound tissue to help the OCS/HA-HClO hydrogel adhere to wounds tightly.

Through the strain sweep of the OCS/HA-HClO hydrogel in Supplementary Figure S2, we observe that the intersection of G′ and G″ curves is approximately 200%, implying that the strain higher than 200% could break the large proportion of crosslinkings inside the OCS/HA-HClO hydrogels. Therefore,

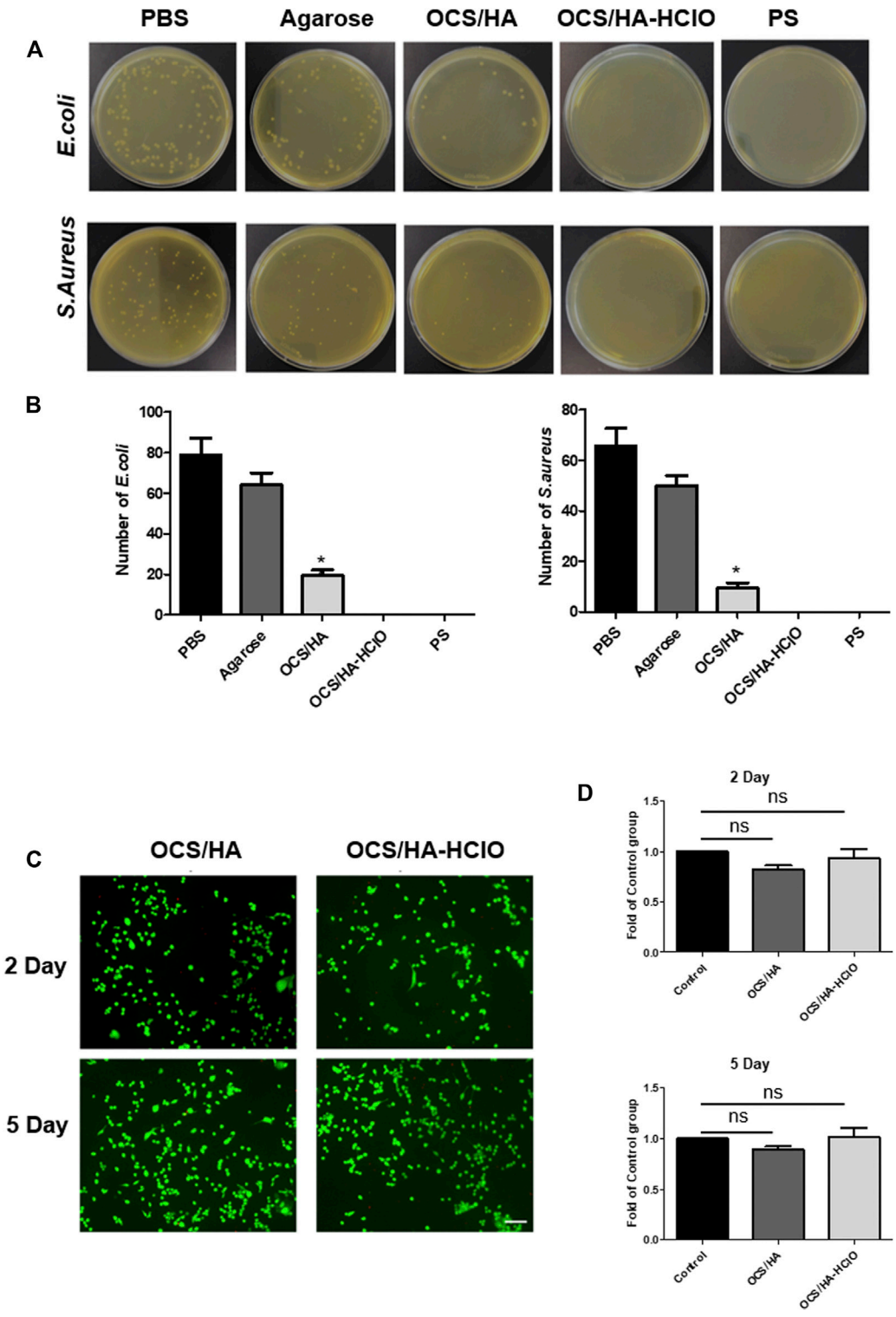

FIGURE 6
Antibacterial performance and biocompatibility of the OCS/HA and OCS/HA-HClO hydrogels. **(A)** Antibacterial performance of hydrogels against *E.coli* and *S.aureus*. **(B)** Quantitative data of A. In this experiment, the PBS group is the blank control; the Agarose group is the negative control; Penicillin-Streptomycin (PS) is the positive control. $p < 0.05$ **(C)** Live/dead staining of 3T3 cells on the surface of the OCS/HA and OCS/HA-HClO hydrogels after 2 d and 5 d of *in vitro* culture, respectively ($n = 4$, scale bar: 100 μm).**(D)** Anti-proliferation effect of the OCS/HA and OCS/HA-HClO hydrogels at 2 d and 5 d. ns: no significant, $p > 0.05$.

we selected 500% as the high train in the subsequent alternating straining sweep test. Figure 4C demonstrates that the OCS/HA-HClO hydrogel has a satisfactory "sol-gel" transition with cyclic changing of the high/low strain. The OCS/HA-HClO hydrogel is transferred to the "sol" state ($G'' > G'$) under the high shear strain and reverts to the original "Gel" state ($G' > G''$) owing to the reversible dynamic crosslinkings in the OCS/HA-HClO hydrogel. The compressive test (Figure 4D) also demonstrates the enhancement of the mechanical properties of the OCS/HA-HClO hydrogel with the increase of the OCS concentration. These strongly indicate that the OCS/HA-HClO hydrogel has a good injection and self-healing property, which is proved in our subsequent studies.

Self-healing, injection, and adhesion performance of the OCS/HA and OCS/HA-HClO hydrogels

The self-healing, injection, and tissue-adhesive properties of hydrogels play a critical role for its application in wound dressing. The photographs in Figure 5A show the injectable behavior of the OCS/HA-HClO hydrogel. The HA-ADH solution dyed using methylene blue is mixed and injected into the left half of the polytetrafluoroethylene (PTFE) mold with the OCS solution. Thereafter, the methylene orange-dyed HA-ADH solution is mixed and injected into the right half of the same mold with the OCS concentration. Finally, the OCS/HA-HClO hydrogel is removed from the PTFE mold and assumes the perfect pentacle shape. These results reveal that the OCS/HA-HClO hydrogel has the ability to match various wound shapes perfectly. Macroscopic photographic evidence of the self-healing behavior is presented in Figure 5B. The cylindrical hydrogel was cut to two semi-cylindrical ones after the compressive test. The compressive test was performed after 1 h of self-healing. As shown in Supplementary Figure S3, there is no significant difference between these two results, indicating the efficient self-healing property of the OCS/HA-HClO hydrogel. The injectability test was performed as described (Makvandi et al., 2019; Makvandi et al., 2021). Two triangle hydrogels, blue and orange, come into contact and become an integrated rhomboid hydrogel after 15 min. The color of the contact interface between these two hydrogels becomes light green, demonstrating the good coalescence between these two triangular hydrogels and indicating their excellent self-healing performance, which is attributed to the reversible dynamic Schiff-base reaction between the hydrazide group of HA-ADH and the aldehyde group of OCS (Figure 5C). Moreover, the OCS/HA-HClO hydrogels exhibit a strong tissue adhesion to wet pig skin, even under sustained folding and twisting (Figure 5D), indicating that after the OCS/HA-HClO hydrogel covers the wound it can adhere to the wound tightly to offer an all-round protection for the wound.

In Vitro antibacterial and biocompatibility of the OCS/HA-HClO hydrogels

Antibacterial resistance to antibiotics, e.g., Penicillin-Streptomycin (PS), has become a global healthcare problem. New strategies against the antibiotic-resistant are urgent to be developed. Numerous articles address the effects of HClO as a treatment for the pathogens and infection. HClO is an effective antimicrobial chemotherapeutic agent which is non-irritating and non-sensitizing due to its less cytotoxicity to eukaryotic cells. It can be generated by the body's immune system to fight invading microbes (Wang et al., 2007). HClO can oxidize the microbial amino acids containing amines and sulfurs, and then cleave to the microbial DNA after it is transformed into a hydroxyl radical (Baek et al., 2020). The *in vitro* antibacterial experiment indicates that the OCS/HA hydrogel has a clear antibacterial effect, which is because of the positive charge in the OCS backbone (Figures 6A,B). Notably, the OCS/HA-HClO hydrogel group reaches 100% bacterial mortality, which is at the same level as the antibiotics PS positive control group. These results demonstrate our assumption for this antibacterial hydrogel that the fresh release of HClO during the OCS/HA-HClO hydrogel formation is responsible for the instant disinfection, whereas the positive charges in the OCS/HA-HClO hydrogel are responsible for the antibacterial effect. We also tested the biocompatibility of the OCS/HA and OCS/HA-HClO hydrogels by using the 3T3 cells as the model cells. The live/dead results in Figure 6C show that the 3T3 cells on the surface of the OCS/HA and OCS/HA-HClO hydrogels remain largely viable with no significant differences to the positive group, indicating the good biocompatibility of the OCS/HA and OCS/HA-HClO hydrogels. Last, we examined the anti-proliferation effect of 3T3 cells with the OCS/HA and OCS/HA-HClO hydrogels or without hydrogel as the control. Compared with the control group, both the OCS/HA and OCS/HA-HClO hydrogel groups demonstrate no significantly suppressed proliferation of the 3T3 cells after 2 d and 5 d (Figure 6D). These results indicate the good biocompatibility of the OCS/HA and OCS/HA-HClO hydrogels.

Conclusion

In conclusion, we present an injectable, self-healing, and tissue adhesive hydrogel mainly based for the convenient and efficient Schiff-base reaction between HA-ADH and OCS. Moreover, during the *in situ* gelation, the HClO originated from the reaction between the predissolved SA and $Ca(ClO)_2$. The hydrogel possesses an outstanding instant sterilization capacity. Meanwhile, the hydrogel is capable of maintaining an antibacterial effect owing to positive charge of OCS. Based on these outstanding properties, the OCS/HA-HClO hydrogel can easily fill and cover the irregular wound, disinfect the wound promptly, and thereafter provide an all-around wound antibacterial protection consistently. This OCS/HA-HClO

hydrogel should be a promising material that can be used for clinical wound dressing.

Data availability statement

The original contributions presented in the study are included in the article/Supplementary Material; further inquiries can be directed to the corresponding authors.

Author contributions

HC and RL carried out the experiments. QD and CL analyzed the data. XX and YS wrote and revised the manuscript. All authors contributed and approved the submitted manuscript.

Funding

This work was supported by the Chengdu Science and Technology Bureau, China (grant no. 2021-YF05-00818-SN).

Conflict of interest

The authors declare that the research was conducted in the absence of any commercial or financial relationships that could be construed as a potential conflict of interest.

Publisher's note

All claims expressed in this article are solely those of the authors and do not necessarily represent those of their affiliated organizations, or those of the publisher, the editors, and the reviewers. Any product that may be evaluated in this article, or claim that may be made by its manufacturer, is not guaranteed or endorsed by the publisher.

Supplementary material

The Supplementary Material for this article can be found online at: https://www.frontiersin.org/articles/10.3389/fmats.2022.935096/full#supplementary-material

References

Abdollahi, Z., Zare, N. E., Salimi, F., Goudarzi, I., Tay, F., Makvandi, P., et al. (2021). Bioactive carboxymethyl starch-based hydrogels decorated with CuO nanoparticles: Antioxidant and antimicrobial properties and accelerated wound healing *in vivo*. *Int. J. Mol. Sci.* 22 (5), 2531. doi:10.3390/ijms22052531

Ahmed, J., Gultekinoglu, M., and Edirisinghe, M. (2020). Bacterial cellulose micro-nano fibres for wound healing applications. *Biotechnol. Adv.* 41, 107549. doi:10.1016/j.biotechadv.2020.107549

Aikawan, T., Ito, S., Shinohara, M., Kaneko, M., Kondo, T., Yuasa, M., et al. (2015). A drug formulation using an alginate hydrogel matrix for efficient oral delivery of the manganese porphyrin-based superoxide dismutase mimic. *Biomater. Sci.* 3 (6), 861–869. doi:10.1039/c5bm00056d

Baek, Y., Kim, J., Ahn, J., Jo, I., Ha, N. C., Ryu, S., et al. (2020). Structure and function of the hypochlorous acid-induced flavoprotein rcla from escherichia coli. *J. Biol. Chem.* 295, 3202–3212. doi:10.1074/jbc.RA119.011530

Bagheri, M., Validi, M., Gholipour, A., Makvandi, P., and Sharifi, E. (2021). Chitosan nanofiber biocomposites for potential wound healing applications: Antioxidant activity with synergic antibacterial effect. *Bioeng. Transl. Med.* 7, e10254. doi:10.1002/btm2.10254

Chandna, S., Thakur, N. S., Kaur, R., and Bhaumik, J. (2020). Lignin-bimetallic nanoconjugate doped pH-responsive hydrogels for laser-assisted antimicrobial photodynamic therapy. *Biomacromolecules* 21 (8), 3216–3230. doi:10.1021/acs.biomac.0c00695

Chen, C. J., Chen, C. C., and Ding, S. J. (2016). Effectiveness of hypochlorous acid to reduce the biofilms on titanium alloy surfaces *in vitro*. *Int. J. Mol. Sci.* 17 (7), 1161. doi:10.3390/ijms17071161

Cho, S. H., Noh, J. R., Cho, M. Y., Go, M. J., Kim, Y. H., Kang, E. S., et al. (2017). An injectable collagen/poly(γ-glutamic acid) hydrogel as a scaffold of stem cells and α-lipoic acid for enhanced protection against renal dysfunction. *Biomater. Sci.* 5 (2), 285–294. doi:10.1039/c6bm00711b

Deng, Y., Hussain, I., Kang, M., Li, K., Yao, F., Liu, S., et al. (2018). Self-recoverable and mechanical-reinforced hydrogel based on hydrophobic interaction with selfhealable and conductive properties. *Chem. Eng. J.* 353, 900–910. doi:10.1016/j.cej.2018.07.187

Derakhshanfar, A., Moayedi, J., Derakhshanfar, G., and Poostforoosh Fard, A. (2019). The role of Iranian medicinal plants in experimental surgical skin wound healing: An integrative review. *Iran. J. Basic Med. Sci.* 22 (6), 590–600. doi:10.22038/ijbms.2019.32963.7873

Du, S., Chen, X., Chen, X., Li, S., Yuan, G., Zhou, T., et al. (2019). Covalent chitosan-cellulose hydrogels via Schiff-Base reaction containing macromolecular microgels for pH-sensitive drug delivery and wound dressing. *Macromol. Chem. Phys.* 220 (23), 1900399. doi:10.1002/macp.201900399

Emami, Z., Ehsani, M., Zandi, M., and Foudazi, R. (2018). Controlling alginate oxidation conditions for making alginate-gelatin hydrogels. *Carbohydr. Polym.* 198, 509–517. doi:10.1016/j.carbpol.2018.06.080

Gaspar-Pintiliescu, A., Stanciuc, A. M., and Craciunescu, O. (2019). Natural composite dressings based on collagen, gelatin and plant bioactive compounds for wound healing: A review. *Int. J. Biol. Macromol.* 38, 854–865. doi:10.1016/j.ijbiomac.2019.07.155

Hu, C., Zhang, F., Kong, Q., Lu, Y., Zhang, B., Wu, C., et al. (2019). Synergistic chemical and photodynamic antimicrobial therapy for enhanced wound healing mediated by multifunctional light-responsive nanoparticles. *Biomacromolecules* 20 (12), 4581–4592. doi:10.1021/acs.biomac.9b01401

Huang, J., Guo, X., Yue, G., Hu, Q., and Wang, L. (2018). Boosting CH3OH production in electrocatalytic CO2 reduction over partially oxidized 5 nm cobalt nanoparticles dispersed on single-layer nitrogen-doped graphene. *ACS Appl. Mat. Interfaces* 10 (51), 44403–44414. doi:10.1021/acsami.8b14822

Jalalvandi, E., Hanton, L. R., and Moratti, S. C. (2017). Schiff-base based hydrogels as degradable platforms for hydrophobic drug delivery. *Eur. Polym. J.* 90, 13–24. doi:10.1016/j.eurpolymj.2017.03.003

Jamaledin, R., Yiu, C. K. Y., Zare, E. N., Niu, L. N., Vecchione, R., Chen, G., et al. (2020). Advances in antimicrobial microneedle patches for combating infections. *Adv. Mat.* 32 (33), e2002129. doi:10.1002/adma.202002129

Jommanee, N., Chanthad, C., and Manokruang, K. (2018). Preparation of injectable hydrogels from temperature and pH responsive grafted chitosan with tuned gelation temperature suitable for tumor acidic environment. *Carbohydr. Polym.* 198, 486–494. doi:10.1016/j.carbpol.2018.06.099

Kim, H., Shin, M., Han, S., Kwon, W., and Hahn, S. K. (2019). Hyaluronic acid derivatives for translational medicines. *Biomacromolecules* 20 (8), 2889–2903. doi:10.1021/acs.biomac.9b00564

Knowles, B. R., Wagner, P., Maclaughlin, S., Higgins, M. J., and Molino, P. J. (2017). Silica nanoparticles functionalized with zwitterionic sulfobetaine siloxane for application as a versatile antifouling coating system. *ACS Appl. Mat. Interfaces* 9 (22), 18584–18594. doi:10.1021/acsami.7b04840

Li, M., Liu, X., Tan, L., Cui, Z., Yang, X., Li, Z., et al. (2018). Noninvasive rapid bacteria-killing and acceleration of wound healing through photothermal/photodynamic/copper ion synergistic action of a hybrid hydrogel. *Biomater. Sci.* 6, 2110–2121. doi:10.1039/C8BM00499D

Liang, Y., Xue, J., Du, B., and Nie, J. (2019). Ultrastiff, tough, and healable ionic-hydrogen bond cross-linked hydrogels and their uses as building blocks to construct complex hydrogel structures. *ACS Appl. Mat. Interfaces* 11 (5), 5441–5454. doi:10.1021/acsami.8b20520

Lin, K., Zhang, D., Macedo, M. H., Cui, W., Sarmento, B., Shen, G., et al. (2019). Advanced collagen-based biomaterials for regenerative biomedicine. *Adv. Funct. Mat.* 29 (3), 1804943. doi:10.1002/adfm.201804943

Litwiniuk, M., Krejner, A., Speyrer, M. S., Gauto, A. R., and Grzela, T. (2016). Hyaluronic acid in inflammation and tissue regeneration. *Wounds*. 28 (3), 78–88.

Makvandi, P., Ali, G. W., Della Sala, F., Abdel-Fattah, W. I., and Borzacchiello, A. (2019). Biosynthesis and characterization of antibacterial thermosensitive hydrogels based on corn silk extract, hyaluronic acid and nanosilver for potential wound healing. *Carbohydr. Polym.* 223, 115023. doi:10.1016/j.carbpol.2019.115023

Makvandi, P., Ashrafizadeh, M., Ghomi, M., Najafi, M., Hossein, H. H. S., Zarrabi, A., et al. (2021). Injectable hyaluronic acid-based antibacterial hydrogel adorned with biogenically synthesized AgNPs-decorated multi-walled carbon nanotubes. *Prog. Biomater.* 10 (1), 77–89. doi:10.1007/s40204-021-00155-6

Park, S. H., Seo, J. Y., Park, J. Y., Ji, Y. B., Kim, K., Choi, H. S., et al. (2019). An injectable, click-crosslinked, cytomodulin-modified hyaluronic acid hydrogel for cartilage tissue engineering. *NPG Asia Mat.* 11 (1), 30. doi:10.1038/s41427-019-0130-1

Pellá, M. C. G., Lima-Tenório, M. K., Tenório-Neto, E. T., Guilherme, M. R., Muniz, E. C., Rubira, A. F., et al. (2018). Chitosan-based hydrogels: From preparation to biomedical applications. *Carbohydr. Polym.* 196, 233–245. doi:10.1016/j.carbpol.2018.05.033

Pérez-Madrigal, M. M., Shaw, J. E., Arno, M. C., Hoyland, J. A., Richardson, S. M., and Dove, A. P. (2020). Robust alginate/hyaluronic acid thiol-yne click-hydrogel scaffolds with superior mechanical performance and stability for load-bearing soft tissue engineering. *Biomater. Sci.* 8 (1), 405–412. doi:10.1039/c9bm01494b

Pupkaite, J., Rosenquist, J., Hilborn, J., and Samanta, A. (2019). Injectable shape-holding collagen hydrogel for cell encapsulation and delivery cross-linked using thiol-michael addition click reaction. *Biomacromolecules* 20 (9), 3475–3484. doi:10.1021/acs.biomac.9b00769

Raval, Y. S., Flurin, L., Mohamed, A., Greenwood-Quaintance, K. E., Beyenal, H., and Patel, R. (2021). *In vitro* activity of hydrogen peroxide and hypochlorous acid generated by electrochemical scaffolds against planktonic and biofilm bacteria. *Antimicrob. Agents Chemother.* 65 (5), AAC.01966-20. doi:10.1128/AAC.01966-20

Rehman, F. U., Jiang, H., Selke, M., and Wang, X. (2018). Mammalian cells: A unique scaffold for *in situ* biosynthesis of metallic nanomaterials and biomedical applications. *J. Mat. Chem. B* 6 (41), 6501–6514. doi:10.1039/c8tb01955j

Shao, C., Chang, H., Wang, M., Xu, F., and Yang, J. (2017). High-strength, tough, and self-healing nanocomposite physical hydrogels based on the synergistic effects of dynamic hydrogen bond and dual coordination bonds. *ACS Appl. Mat. Interfaces* 9 (34), 28305–28318. doi:10.1021/acsami.7b09614

Shariatinia, Z. (2019). Pharmaceutical applications of chitosan. *Adv. Colloid Interface Sci.* 263, 131–194. doi:10.1016/j.cis.2018.11.008

Smithmyer, M. E., Sawicki, L. A., and Kloxin, A. M. (2014). Hydrogel scaffolds as *in vitro* models to study fibroblast activation in wound healing and disease. *Biomater. Sci.* 2 (5), 634–650. doi:10.1039/C3BM60319A

Tian, S., Jiang, D., Pu, J., Sun, X., Li, Z., Wu, B., et al. (2019). A new hybrid silicone-based antifouling coating with nanocomposite hydrogel for durable antifouling properties. *Chem. Eng. J.* 370, 1–9. doi:10.1016/j.cej.2019.03.185

Vimbela, G. V., Ngo, S. M., Fraze, C., Yang, L., and Stout, D. A. (2017). Antibacterial properties and toxicity from metallic nanomaterials. *Int. J. Nanomedicine* 12, 3941–3965. doi:10.2147/IJN.S134526

Wakuda, Y., Nishimoto, S., Suye, S. I., and Fujita, S. (2018). Native collagen hydrogel nanofibres with anisotropic structure using core-shell electrospinning. *Sci. Rep.* 8 (1), 6248. doi:10.1038/s41598-018-24700-9

Wang, L., Bassiri, M., Najafi, R., Najafi, K., Yang, J., Khosrovi, B., et al. (2007). Hypochlorous acid as a potential wound care agent. Part I. Stabilized hypochlorous acid: A component of the inorganic armamentarium of innate immunity. *J. Burns Wounds* 6, 65.

Wang, H., Qian, J., and Ding, F. (2018). Emerging chitosan-based films for food packaging applications. *J. Agric. Food Chem.* 66 (2), 395–413. doi:10.1021/acs.jafc.7b04528

Wang, J., Wang, L., Wu, C., Pei, X., Cong, Y., Zhang, R., et al. (2020). Antibacterial zwitterionic polyelectrolyte hydrogel adhesives with adhesion strength mediated by electrostatic mismatch. *ACS Appl. Mat. Interfaces* 12 (41), 46816–46826. doi:10.1021/acsami.0c14959

Wang, Y., Xie, R., Li, Q., Dai, F., Lan, G., Shang, S., et al. (2020). A self-adapting hydrogel based on chitosan/oxidized konjac glucomannan/AgNPs for repairing irregular wounds. *Biomater. Sci.* 8 (7), 1910–1922. doi:10.1039/c9bm01635j

Wolf, K. J., and Kumar, S. (2019). Hyaluronic acid: Incorporating the bio into the material. *ACS Biomater. Sci. Eng.* 5 (8), 3753–3765. doi:10.1021/acsbiomaterials.8b01268

Zhang, X., Zhao, G., Cao, Y., Haider, Z., Wang, M., Fu, J., et al. (2018). Magnetothermal heating facilitates the cryogenic recovery of stem cell-laden alginate-Fe_3O_4 nanocomposite hydrogels. *Biomater. Sci.* 6 (12), 3139–3151. doi:10.1039/c8bm01004h

Zhang, S., Ou, Q., Xin, P., Yuan, Q., Wang, Y., Wu, J., et al. (2019). Polydopamine/puerarin nanoparticle-incorporated hybrid hydrogels for enhanced wound healing. *Biomater. Sci.* 7 (10), 4230–4236. doi:10.1039/c9bm00991d

Zhu, Q., Jiang, M., Liu, Q., Yan, S., Feng, L., Lan, Y., et al. (2018). Enhanced healing activity of burn wound infection by a dextran-HA hydrogel enriched with sanguinarine. *Biomater. Sci.* 6 (9), 2472–2486. doi:10.1039/c8bm00478a